Spectroscopic and Electrical Properties of $[Fe(C_3X_5)_2]^-$ (X = S or Se) Complexes and Crystal Structures of $[NBu^n_4][Fe(C_3S_5)_2]$ and $[Fe(C_5Me_5)_2][Fe(C_3S_5)_2]$†

Satoshi Tanaka and Gen-etsu Matsubayashi*
Institute of Chemistry, College of General Education, Osaka University, Toyonaka, Osaka 560, Japan

Complexes containing the $[Fe(C_3S_5)_2]^-$ anion [$C_3S_5^{2-}$ = 4,5-dimercapto-1,3-dithiole-2-thionate(2−)] and $[Fe(C_3Se_5)_2]^-$ [$C_3Se_5^{2-}$ = 4,5-di(hydroseleno)-1,3-diselenole-2-selonate(2−)] have been prepared. Single-crystal X-ray analyses of the $[NBu^n_4]^+$ and $[Fe(C_5Me_5)_2]^+$ salts of $[Fe(C_3Se_5)_2]^-$ revealed dimerized geometries for the anions with square-pyramidal co-ordination around each Fe^{III} through intermolecular Fe–S linkages. One-dimensional arrays of the dimerized anion moieties are built up *via* weak sulfur–sulfur non-bonded contacts in the crystal phases. The crystals of both complexes are triclinic, space group $P\bar{1}$, with cell parameters a = 11.969(3), b = 14.249(3), c = 9.965(2) Å, α = 102.95(2), β = 97.71(2), γ = 80.95(2)°, and Z = 2 for the $[NBu^n_4]^+$ salt and a = 15.416(3), b = 15.976(3), c = 16.106(4) Å, α = 93.32(2), β = 101.41(2), γ = 56.60(1)°, and Z = 4 for the $[Fe(C_5Me_5)_2]^+$ salt. Least-squares refinements, based on 3770 and 7069 reflections [$|F_o| > 3\sigma(F)$] converged at R = 0.075 and 0.067, respectively. The complexes were oxidized upon treatment with iodine, $[ttf]_3[BF_4]_2$ ($ttf^{\cdot+}$ = the radical cation of tetrathiafulvalene), $[Fe(C_5H_5)_2][PF_6]$, or $[Fe(C_5Me_5)_2][BF_4]$ and by current-controlled electrolysis to afford partially oxidized $[Fe(C_3S_5)_2]^{n-}$ and $[Fe(C_3Se_5)_2]^{n-}$ (n = 0.05–0.7) species. The oxidized C_3S_5 complexes exhibit electrical conductivities of 1.9 × 10^{-5}–1.0 × 10^{-1} S cm^{-1} and the oxidized C_3Se_5 complexes 5.9 × 10^{-8}–1.1 × 10^{-2} S cm^{-1} at room temperature as compacted pellets. Ligand-centred oxidation is deduced to occur for the partially oxidized complexes on the basis of IR, ESR, and X-ray photoelectron spectra.

Metal complexes with the sulfur-rich ligand $C_3S_5^{2-}$ [4,5-dimercapto-1,3-dithiole-2-thionate(2−)] have been studied from the standpoint that they may have the potential to become electrical conductors having electron-conduction pathways through S···S molecular interactions.[1,2] Bis[dithiolato(2−)]-iron(III) anion complexes are known to have dimerized anion structures through Fe–S interactions in the solid state.[3–7] Similarly, complexes of $[Fe(C_3X_5)_2]^-$ (X = S or Se) and their oxidized species are expected to display packing modes of the anion moieties due to S···S intermolecular interactions in the solid state, so forming effective electrical conduction pathways. Previously, $[NBu^n_4][Fe(C_3S_5)_2]$ has been prepared and electrical conductivities of some oxidized $[Fe(C_3S_5)_2]^{n-}$ (n < 1) anion species were measured.[8–10] However, little is known of the structures and properties of these species. Furthermore, the C_3Se_5 analogues are also of much interest, since even more effective molecular interactions are expected to occur owing to selenium having more extended orbitals than sulfur.[11] This paper reports spectroscopic properties of $[Fe(C_3X_5)_2]^-$ (X = S or Se) anion complexes and electrical conductivities of their oxidized species. Crystal structures of $[NBu^n_4][Fe(C_3S_5)_2]$ and $[Fe(C_5Me_5)_2][Fe(C_3S_5)_2]$ are also described.

Experimental

Preparations.—$[NBu^n_4][Fe(C_3S_5)_2]$ **1** *and* $[NMe_4][Fe(C_3S_5)_2]$ **2**. All the following reactions were performed under a nitrogen atmosphere. 4,5-Bis(benzoylthio)-1,3-dithiole-2-thione[12] (200 mg, 490 μmol) was dissolved in a methanol (15 cm^3) solution containing sodium metal (25 mg, 1.1 mmol). To the resulting solution of $Na_2[C_3S_5]$ was added with stirring a methanol (5 cm^3) solution containing $FeCl_3$ (40 mg, 250 μmol) and $[NBu^n_4]Br$ (120 mg, 370 μmol). Immediately dark brown solids of complex **1** precipitated, which were filtered off, washed with water, methanol and diethyl ether, and dried *in vacuo* (70% yield). They were recrystallized from acetonitrile to afford black crystals suitable for X-ray structure analysis. A similar reaction, using $[NMe_4]Br$ instead of $[NBu^n_4]Br$, afforded black microcrystals of $[NMe_4][Fe(C_3S_5)_2]$ **2** (58% yield).

$[ttf][Fe(C_3S_5)_2]$ **3**. An acetonitrile (20 cm^3) solution of complex **1** (20 mg, 29 μmol) was added with stirring to an acetonitrile (10 cm^3) solution of $[ttf]_3[BF_4]_2$[13] (35 mg, 44 μmol) [ttf = tetrathiafulvalene = 2-(1′,3′-dithiol-2′-ylidene)-1,3-dithiole]. Immediately black solids of complex **3** precipitated, which were filtered off, washed with acetonitrile, and dried *in vacuo* (81% yield). The presence of the $ttf^{\cdot+}$ radical cation was confirmed by ESR spectroscopy.

$[Fe(C_5Me_5)_2][Fe(C_3S_5)_2]$ **4**. An acetonitrile (20 cm^3) solution of complex **1** (20 mg, 29 μmol) was added with stirring to an acetonitrile (2.5 cm^3) solution of $[Fe(C_5Me_5)_2][BF_4]$[14] (35 mg, 85 μmol) to yield immediately black solids of complex **4** (80% yield). Diffusion of complex **1** (20 mg, 29 μmol) and $[Fe(C_5Me_5)_2][BF_4]$ (12 mg, 29 μmol) in aceonitrile (50 cm^3), using a conventional H-tube cell set in a thermostatted (40 °C) dark chamber for 30 d, afforded black crystals of **4** (5 mg), which were suitable for X-ray structure analysis.

$[NBu^n_4][Fe(C_3Se_5)_2]$ **5** *and* $[NMe_4][Fe(C_3Se_5)_2]$ **6**. 4,5-Bis-(benzoylseleno)-1,3-diselenole-2-selone[15] (315 mg, 490 μmol) was dissolved in a methanol (15 cm^3) solution containing sodium metal (25 mg, 1.1 mmol). To the resulting solution of $Na_2[C_3Se_5]$ was added $[NBu^n_4]Br$ (120 mg, 370 μmol), followed by addition of a methanol (5 cm^3) solution of $FeCl_3$ (40 mg, 245 μmol). Black solids of complex **5** precipitated, which were filtered off, washed with water, methanol and diethyl ether, and dried *in vacuo* (95% yield). Similarly, black solids of complex **6** were prepared by using $[NMe_4]Br$ instead of $[NBu^n_4]Br$ (82% yield).

† *Supplementary data available:* see Instructions for Authors, *J. Chem. Soc., Dalton Trans.*, 1992, Issue 1, pp. xx–xxv.
Non-SI unit employed: eV ≈ 1.60 × 10^{-19} J.

Table 1 Elemental analysis of the $[Fe(C_3X_5)_2]^{n-}$ (X = S or Se; n = 0.05–1) complexes

Complex	Analysis (%)* H	C	N	S
1 $[NBu^n_4][Fe(C_3S_5)_2]$	5.1 (5.2)	38.5 (38.25)	1.95 (2.0)	46.3 (46.4)
2 $[NMe_4][Fe(C_3S_5)_2]$	2.2 (2.3)	22.8 (23.0)	2.75 (2.65)	60.5 (61.35)
3 $[ttf][Fe(C_3S_5)_2]$	0.55 (0.6)	21.8 (22.05)		67.5 (68.75)
4 $[Fe(C_5Me_5)_2][Fe(C_3S_5)_2]$	3.9 (3.9)	39.9 (40.3)		40.4 (41.4)
5 $[NBu^n_4][Fe(C_3Se_5)_2]$	3.15 (3.1)	22.45 (22.8)	1.15 (1.2)	
6 $[NMe_4][Fe(C_3Se_5)_2]$	1.45 (1.2)	12.05 (12.1)	1.3 (1.4)	
7 $[NBu^n_4]_{0.05}[Fe(C_3S_5)_2]$	0.5 (0.4)	17.6 (17.7)	0.55 (0.2)	
8 $[NBu^n_4]_{0.33}[Fe(C_3S_5)_2]$	2.1 (2.1)	23.25 (24.9)	0.95 (0.8)	
9 $[NMe_4]_{0.4}[Fe(C_3S_5)_2]$	1.1 (1.0)	18.7 (19.1)	1.25 (1.15)	
10 $[ttf]_{0.28}[Fe(C_3Se_5)_2]$	0.1 (0.1)	9.5 (9.45)		
11 $[Fe(C_5Me_5)_2]_{0.7}[Fe(C_3Se_5)_2]$	1.95 (1.85)	20.45 (20.95)		
12 $[NBu^n_4]_{0.05}[Fe(C_3Se_5)_2]$	0.0 (0.15)	9.1 (8.8)	0.0 (0.05)	
13 $[NBu^n_4]_{0.66}[Fe(C_3S_5)_2]$	3.95 (3.65)	31.1 (31.55)	1.4 (1.4)	
14 $[NMe_4]_{0.53}[Fe(C_3S_5)_2]$	1.35 (1.3)	19.85 (20.0)	1.5 (1.5)	

* Calculated values in parentheses.

Table 2 Experimental data and structure refinement details[a] for complexes **1** and **4**

Complex	**1**	**4**
Formula	$C_{22}H_{36}FeNS_{10}$	$C_{26}H_{30}Fe_2S_{10}$
M	691.0	774.9
Crystal size/mm	0.10 × 0.35 × 0.40	0.15 × 0.22 × 0.50
a/Å	11.969(3)	15.416(3)
b/Å	14.249(3)	16.976(3)
c/Å	9.965(2)	16.106(4)
α/°	102.95(2)	93.32(2)
β/°	97.71(2)	101.41(2)
γ/°	80.95(2)	56.60(1)
U/Å^3	1627.0(6)	3240(1)
D_c/g cm^{-3}	1.410(1)	1.589(1)
F(000)	722.0	1592.0
Radiation (λ/Å)	Mo-Kα (0.710 69)	Cu-Kα (1.5418)
μ/cm^{-1}	10.9	132.1
Scan interval/° min^{-1}	8	4
Collected octants	$+h, \pm k, \pm l$	$+h, \pm k, \pm l$
No. of data collected at room temperature	7451	10 032
No. of independent data with $\|F_o\| > 3\sigma(F)$	3770	7069
Absorption correction range[b]	1.00–0.86	1.00–0.49
R	0.075	0.067
R'	0.096[c]	0.075[d]

[a] Rigaku-AFC diffractometer; for complex **1**, triclinic, space group $P\bar{1}$, Z = 2, scan range $3 < 2\theta < 55°$ and for complex **4**, triclinic, space group $P\bar{1}$, Z = 4, scan range $4 < 2\theta < 120°$. [b] See ref. 19. [c] $\Sigma w(|F_o| - |F_c|)^2$, where $w = 4F_o^2/\sigma^2(F_o^2)$. [d] $[\Sigma w(|F_o| - |F_c|)^2/\Sigma w|F_o|^2]^{\frac{1}{2}}$, where $w^{-1} = \sigma^2(F_o) + 0.000\,05F_o^2$.

Partially oxidized $[Fe(C_3S_5)_2]^{n-}$ *and* $[Fe(C_3Se_5)_2]^{n-}$ ($n < 1$) *complexes by reactions with oxidants.* To an acetonitrile (20 cm^3) solution of complex **1** (20 mg, 29 μmol) was added an acetonitrile (2.5 cm^3) solution of $[Fe(C_5H_5)_2][PF_6]$[16] (19 mg, 58 μmol). Immediately brown solids of $[NBu^n_4]_{0.05}[Fe(C_3S_5)_2]$ **7** precipitated, which were collected by filtration, washed with acetonitrile and dried *in vacuo* (78% yield). Treatment of complex **1** (29 mg, 30 μmol) or **2** (16 mg, 30 μmol) with iodine (12 mg, 90 μmol) in acetonitrile (25 cm^3) afforded brown solids of $[NBu^n_4]_{0.33}[Fe(C_3S_5)_2]$ **8** (56% yield) or black solids of $[NMe_4]_{0.4}[Fe(C_3S_5)_2]$ **9** (84% yield). Reaction of complex **5** (20 mg, 17 μmol) with $[ttf]_3[BF_4]_2$ (27 mg, 34 μmol) in acetonitrile (30 cm^3) yielded black solids of $[ttf]_{0.3}[Fe(C_3Se_5)_2]$ **10** (94% yield). Similarly, reaction of complex **5** (30 mg, 26 μmol) with $[Fe(C_5Me_5)_2][BF_4]$ (27 mg, 65 μmol) or $[Fe(C_5H_4Me)_2][PF_6]$[16] (23 mg, 65 μmol) in acetonitrile (30 cm^3) afforded black solids of $[Fe(C_5Me_5)_2]_{0.7}[Fe(C_3Se_5)_2]$ **11** (95% yield) or $[NBu^n_4]_{0.05}[Fe(C_3Se_5)_2]$ **12** (90% yield).

Partially oxidized $[Fe(C_3S_5)_2]^{n-}$ *and* $[Fe(C_3Se_5)_2]^{n-}$ ($n < 1$) *complexes by electrolysis.* An acetonitrile (50 cm^3) solution containing complex **1** (20 mg, 29 μmol) and $[NBu^n_4][ClO_4]$ (1.0 g, 3 mmol) was subjected to a controlled-current (1 μA) electrolysis at 30 °C for 15 d in an H-type glass cell consisting of platinum wire electrodes. Black microcrystals of $[NBu^n_4]_{0.66}[Fe(C_3S_5)_2]$ **13** produced on the anode were collected and dried *in vacuo* (yield 3 mg). Similarly, black microcrystals of $[NMe_4]_{0.53}[Fe(C_3S_5)_2]$ **14** were also obtained by the galvanostatic electrolysis (current 1 μA) of an acetonitrile (50 cm^3) solution containing complex **2** (20 mg, 38 μmol) and $[NMe_4][ClO_4]$ (520 mg, 3 mmol) at 30 °C for 20 d (4 mg yield).

Elemental analyses for the complexes obtained are given in Table 1.

Physical Measurements.—Electrical conductivities of the complexes were measured for compacted pellets at room temperature by the conventional two-probe method.[16] Electronic absorption, powder reflectance,[17] IR,[16] ESR, and X-ray photoelectron spectra (XPS)[18] were recorded as described previously. Cyclic voltammograms were measured for complexes dissolved in a dimethylformamide solution containing $[NBu^n_4][ClO_4]$ as a supporting electrolyte, using a conventional cell consisting of two platinum plates as working and counter electrodes and a saturated calomel electrode (SCE) as a reference.

X-Ray Crystal-structure Determinations of $[NBu^n_4][Fe(C_3S_5)_2]$ **1** *and* $[Fe(C_5Me_5)_2][Fe(C_3S_5)_2]$ **4**.—Crystal data and details of the measurements are listed in Table 2. The unit-cell parameters were determined from 25 independent reflections with 2θ values in the range 24.5–25° (Mo-Kα radiation) for complex **1** and 43–65° (Cu-Kα radiation) for complex **4**.

The structure of complex **1** was solved by direct methods.[20] All the calculations were performed using the TEXSAN crystallographic software package of Molecular Structure Corporation.[21] The non-hydrogen atoms were refined anisotropically by full-matrix least-squares refinement. The structure of complex **4** was also solved according to the direct (MULTAN) method.[22] Subsequent Fourier maps revealed the positions of all the non-hydrogen atoms, which were refined anisotropically by block-diagonal least squares. Atomic scattering factors used in the refinement were taken from ref. 23. Crystallographic calculations were performed using the programs of Professor K. Nakatsu, Kwansei Gakuin University, on an ACOS 930S computer at the Research Center of Protein Engineering, Institute for Protein Research, Osaka University.

Atomic coordinates for complexes **1** and **4** are in Tables 3 and 4, respectively. Figs. 1–4 were drawn with a local version of ORTEP II.[24]

Additional material available from the Cambridge Crystallographic Data Centre comprises H-atom coordinates, thermal parameters and remaining bond lengths and angles.

Table 3 Atomic coordinates for $[NBu^n_4][Fe(C_3S_5)_2]$ **1** with estimated standard deviations (e.s.d.s) in parentheses

Atom	*x*	*y*	*z*
Fe	0.4664(2)	0.1141(1)	0.5233(2)
S(1)	0.3993(3)	0.0069(3)	0.6161(3)
S(2)	0.1883(3)	−0.0961(3)	0.5361(4)
S(3)	−0.0156(3)	−0.1533(3)	0.3512(4)
S(4)	0.1146(3)	−0.0024(3)	0.3062(4)
S(5)	0.3124(3)	0.1160(3)	0.3689(4)
S(6)	0.5637(3)	0.1567(3)	0.7322(3)
S(7)	0.7429(3)	0.2934(3)	0.8293(4)
S(8)	0.8831(4)	0.4408(3)	0.7979(6)
S(9)	0.6980(4)	0.3715(3)	0.5817(5)
S(10)	0.5129(4)	0.2423(3)	0.4577(4)
N	0.2546(9)	0.2624(8)	0.0989(10)
C(1)	0.269(1)	−0.012(1)	0.514(1)
C(2)	0.090(1)	−0.089(1)	0.396(1)
C(3)	0.236(1)	0.032(1)	0.406(1)
C(4)	0.635(1)	0.247(1)	0.709(1)
C(5)	0.782(1)	0.374(1)	0.740(2)
C(6)	0.615(1)	0.284(1)	0.593(2)
C(7)	0.261(1)	0.266(1)	0.836(1)
C(8)	0.207(1)	0.361(1)	0.797(1)
C(9)	0.222(1)	0.351(1)	0.644(1)
C(10)	0.165(2)	0.441(1)	0.590(2)
C(11)	0.312(1)	0.162(1)	1.011(1)
C(12)	0.246(1)	0.077(1)	0.950(1)
C(13)	0.321(1)	−0.017(1)	0.971(1)
C(14)	0.255(2)	−0.104(1)	0.927(2)
C(15)	0.312(1)	0.343(1)	1.088(1)
C(16)	0.439(1)	0.336(1)	1.072(2)
C(17)	0.485(2)	0.425(2)	1.176(2)
C(18)	0.595(2)	0.423(2)	1.187(3)
C(19)	0.128(1)	0.282(1)	1.016(1)
C(20)	0.108(1)	0.272(1)	1.162(1)
C(21)	−0.021(1)	0.285(1)	1.164(2)
C(22)	−0.049(1)	0.276(1)	1.306(2)

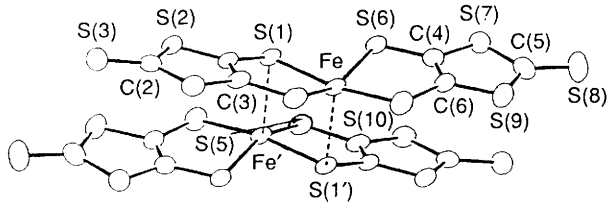

Fig. 1 Molecular geometry of the anion moieties of $[NBu^n_4][Fe(C_3S_5)_2]$ **1**, together with the atom-labelling scheme

Results and Discussion

Crystal Structures of $[NBu^n_4][Fe(C_3S_5)_2]$ **1** *and* $[Fe(C_5Me_5)_2][Fe(C_3S_5)_2]$ **4**.—Fig. 1 illustrates the geometry of the anion of complex **1**, together with the atom-labelling scheme (in which primed atoms are related to unprimed atoms by a centre of symmetry). Selected bond distances and angles of the anion are listed in Table 5. The iron(III) ion is co-ordinated to four sulfur atoms of the two planar $C_3S_5^{2-}$ ligands and with a fifth sulfur atom of another anion so adopting a square-pyramidal geometry. The dihedral angle between the two $C_3S_5^{2-}$ ligands is 11.85 . The Fe–S bond distances in the anion range from 2.238 to 2.250 Å, while the distance between the iron atom and the axial sulfur atom, S(1′), from the neighbouring anion is somewhat longer (2.478 Å). The structural characteristics are very close to those of $[NBu^n_4]_2[Fe_2\{S_2C_2(CN)_2\}_4]$ [Fe–S_{ax} 2.460(7) Å],[3] $[NBu^n_4]_2[Fe_2(S_2C_2H_4)_4]$ [2.503(3) Å][4] and $[NBu^n_4]_2[Fe_2(S_2C_6H_3Me\text{-}4)_4]$ [2.51(5) Å].[7] These complexes also assume square-pyramidal geometries except for $[NBu^n_4]_2[Fe_2(S_2C_2H_4)_4]$ which is trigonal bipyramidal. The Fe···Fe distance in **1** is considerably short (3.17 Å), which results in a strong antiferromagnetic interaction between the metal centres as described below. Fig. 2 shows the molecular packing of the

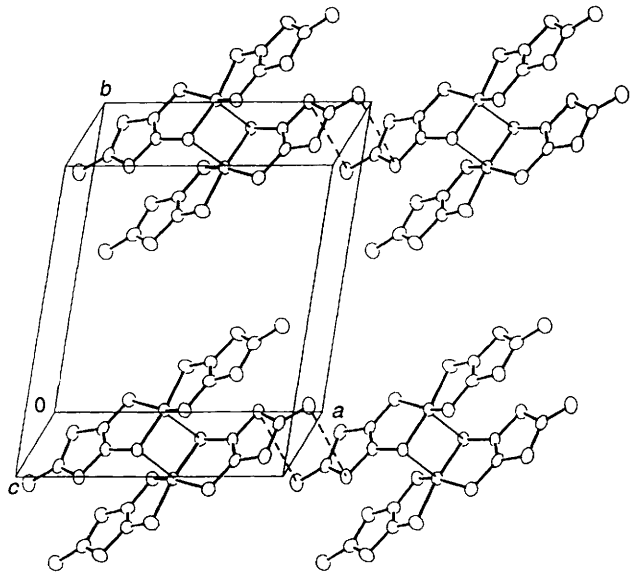

Fig. 2 Packing diagram of the anions of $[NBu^n_4][Fe(C_3S_5)_2]$ **1**; dashed lines represent non-bonded S···S contacts less than 4.0 Å

anions in the unit cell of complex **1**. The dimerized anion units form a one-dimensional array approximately along the *a* axis through weak S···S non-bonded contacts. Such a chain structure of the anions with S···S non-bonded contacts has been found previously in other C_3S_5–metal complexes: $[NBu^n_4][Au(C_3S_5)_2]$,[11] $[Fe(C_5Me_5)_2][Au(C_3S_5)_2]$,[25] and $[EtNC_5H_5]_2[Cu(C_3S_5)_2]$.[26]

The crystal structure of complex **4** consists of two crystallographically independent cations as well as two independent anions. Fig. 3 illustrates the geometries of both the $[Fe(C_5Me_5)_2]^+$ cations and the $[Fe(C_3S_5)_2]^-$ anions, together with the atom-labelling scheme. Selected bond distances and angles are in Table 6. The C_5 rings of the C_5Me_5 moieties of one $[Fe(C_5Me_5)_2]^+$ cation are rotated by approximately 21.6° away from the ideal D_{5h} symmetry, which is rather close to the essentially staggered forms (36° twist angle) observed for the $[Fe(C_5Me_5)_2]^+$ salts of $[C_3(CN)_5]^-$, $[(NC)_2C_2(CN)_2]^-\cdot$ MeCN,[27] $[C_4(CN)_6]^-$,[28] and $[C_6Cl_2(CN)_2(O)(OH)]^-$.[29] On the other hand, the twist angle of the C_5 rings of the other $[Fe(C_5Me_5)_2]^+$ cation is very small (approximately 6.4°), as observed for $[Fe(C_5Me_5)_2]^+$ salts of $[(NC)_2CC_6H_2I_2C(CN)_2]^-$ (4° twist)[30] and $[Au(C_3S_5)_2]^-$ (14° twist).[25] The Fe–C, C–C and C–Me bond distances are in the range 2.066–2.116, 1.40–1.46 and 1.49–1.55 Å and average 2.094, 1.425 and 1.525 Å, respectively. These values are in good agreement with those of the above-mentioned $[Fe(C_5Me_5)_2]^+$ compounds. Atoms Fe(1) and Fe(2) atoms are located at an average distance of 1.704 and 1.709 Å, respectively from the C_5 rings. The Fe–C and Fe–C_5 ring centroid distances are slightly longer than found in $[Fe(C_5Me_5)_2]$ [average 2.050(2) and 1.657 Å, respectively],[31] the C–C and C–Me distances remaining essentially the same.

The anions form dimeric units related by imposed centres of symmetry. The bridging atoms Fe(1)–S(1)–Fe(1′)–S(1′) and Fe(2)–S(11)–Fe(2′)–S(11′) are necessarily coplanar. Each of the iron atoms has a tetragonal-pyramidal geometry. The Fe(1) and Fe(2) atoms lie 0.359 and 0.338 Å above the least-squares planes defined by S(1), S(5), S(6), S(10) and by S(11), S(15), S(16), S(20) atoms, respectively. The dihedral angles between the planes formed by S(1)–S(5) and by S(6)–S(10) around Fe(1) and between those formed by S(11)–S(15) and by S(16)–S(20) around Fe(2) are 12.2 and 11.6°, respectively. The average Fe(1)–S and Fe(2)–S distance is 2.242 Å. The axial positions around Fe(1) and Fe(2) are occupied by S(1′) and S(11′) with Fe–S bond lengths of 2.500(3) and 2.491(3) Å. Fe(1)···Fe(1′) and Fe(2)···Fe(2′) distances are also short [3.169(3) and

Table 4 Fractional atomic coordinates for $[Fe(C_5Me_5)_2][Fe(C_3S_5)_2]$ **4** with e.s.d.s in parentheses

Atom	*x*	*y*	*z*	Atom	*x*	*y*	*z*
Fe(1)	0.071 6(1)	0.382 38(9)	0.492 74(7)	C(23)	0.425 1(7)	0.247 9(7)	0.438 3(6)
Fe(2)	0.397 9(1)	0.106 48(9)	−0.035 24(7)	C(24)	0.416 9(7)	0.250 9(7)	0.346 5(6)
Fe(3)	0.573 4(1)	0.189 07(9)	0.404 70(7)	C(25)	0.450 8(8)	0.312 7(8)	0.327 1(5)
Fe(4)	0.904 9(1)	0.323 68(9)	0.073 71(7)	C(26)	0.668 0(7)	0.034 6(7)	0.388 4(6)
S(1)	0.123 3(2)	0.487 2(2)	0.537 4(1)	C(27)	0.686 6(7)	0.089 3(7)	0.336 3(5)
S(2)	0.202 0(2)	0.587 6(2)	0.446 7(1)	C(28)	0.727 2(7)	0.141 0(7)	0.389 4(5)
S(3)	0.249 0(3)	0.640 2(2)	0.294 2(2)	C(29)	0.727 6(6)	0.120 0(7)	0.475 4(5)
S(4)	0.174 9(2)	0.502 7(2)	0.289 0(1)	C(30)	0.692 6(7)	0.056 2(7)	0.475 8(5)
S(5)	0.107 1(2)	0.383 7(2)	0.365 1(1)	C(31)	0.517 6(11)	0.417 5(9)	0.411 8(9)
S(6)	0.056 5(2)	0.253 6(2)	0.453 9(1)	C(32)	0.483 1(10)	0.329 4(9)	0.562 9(6)
S(7)	0.031 7(2)	0.116 3(2)	0.555 4(1)	C(33)	0.395 3(10)	0.195 9(10)	0.492 6(9)
S(8)	0.023 8(2)	0.037 3(2)	0.714 9(2)	C(34)	0.371 6(9)	0.200 1(11)	0.286 3(10)
S(9)	0.080 4(2)	0.187 6(2)	0.714 7(1)	C(35)	0.449 4(11)	0.341 2(10)	0.237 7(7)
S(10)	0.111 7(2)	0.331 8(2)	0.629 3(1)	C(36)	0.630 4(9)	−0.035 2(7)	0.359 6(7)
S(11)	0.461 6(2)	0.039 5(2)	0.098 3(1)	C(37)	0.674 9(8)	0.087 9(8)	0.239 9(5)
S(12)	0.400 9(2)	−0.065 3(2)	0.204 3(1)	C(38)	0.761 7(9)	0.205 3(8)	0.362 2(7)
S(13)	0.285 5(3)	−0.159 9(2)	0.226 5(1)	C(39)	0.766 4(8)	0.158 1(9)	0.554 5(6)
S(14)	0.243 8(3)	−0.051 3(2)	0.064 4(1)	C(40)	0.687 8(8)	0.010 4(8)	0.554 2(6)
S(15)	0.279 0(2)	0.064 5(2)	−0.052 3(1)	C(41)	0.756 1(6)	0.379 1(6)	0.103 6(5)
S(16)	0.462 9(2)	0.200 2(2)	0.008 9(1)	C(42)	0.742 3(7)	0.424 6(6)	0.023 6(5)
S(17)	0.484 0(2)	0.341 4(2)	−0.090 5(2)	C(43)	0.793 4(6)	0.476 9(6)	0.037 6(5)
S(18)	0.450 0(3)	0.455 8(2)	−0.245 3(2)	C(44)	0.839 7(7)	0.465 2(6)	0.126 0(5)
S(19)	0.352 4(2)	0.338 5(2)	−0.243 1(1)	C(45)	0.817 6(7)	0.402 6(6)	0.167 6(5)
S(20)	0.313 5(2)	0.199 1(2)	−0.158 3(1)	C(46)	1.016 6(7)	0.262 7(6)	−0.004 8(5)
C(1)	0.158 2(6)	0.507 6(6)	0.448 3(4)	C(47)	1.067 6(7)	0.256 6(6)	0.080 8(5)
C(2)	0.211 0(8)	0.579 9(7)	0.340 0(6)	C(48)	1.051 8(7)	0.198 3(6)	0.131 1(5)
C(3)	0.149 9(6)	0.464 6(6)	0.375 5(5)	C(49)	0.989 2(8)	0.167 7(6)	0.076 8(6)
C(4)	0.060 1(6)	0.207 0(6)	0.549 9(5)	C(50)	0.970 1(8)	0.206 3(6)	−0.007 1(5)
C(5)	0.044 0(7)	0.108 9(6)	0.664 5(5)	C(51)	0.708 4(9)	0.321 9(8)	0.118 6(6)
C(6)	0.082 2(7)	0.239 7(6)	0.625 0(5)	C(52)	0.676 0(8)	0.424 6(9)	−0.060 4(5)
C(11)	0.380 8(6)	−0.000 7(5)	0.109 8(4)	C(53)	0.793 0(8)	0.541 1(7)	−0.029 5(6)
C(12)	0.308 3(6)	−0.095 0(7)	0.169 1(5)	C(54)	0.900 3(8)	0.511 0(7)	0.168 4(6)
C(13)	0.306 6(6)	0.006 2(6)	0.045 5(5)	C(55)	0.846 9(8)	0.375 1(7)	0.260 0(5)
C(14)	0.431 9(7)	0.269 7(6)	−0.084 3(5)	C(56)	1.018 2(9)	0.313 5(8)	−0.080 1(6)
C(15)	0.428 3(7)	0.383 4(7)	−0.195 3(5)	C(57)	1.135 6(8)	0.298 7(8)	0.112 8(7)
C(16)	0.369 1(7)	0.268 2(6)	−0.155 2(5)	C(58)	1.097 5(9)	0.166 4(8)	0.225 5(5)
C(21)	0.478 4(8)	0.346 3(7)	0.402 0(6)	C(59)	0.958 4(10)	0.100 1(8)	0.102 2(8)
C(22)	0.465 9(7)	0.305 1(7)	0.469 8(5)	C(60)	0.911 8(10)	0.189 0(8)	−0.087 9(6)

Table 5 Selected bond lengths (Å) and angles (°) with e.s.d.s in parentheses for the anion of $[NBu^n_4][Fe(C_3S_5)_2]$ **1**

Fe–S(1)	2.248(4)	S(5)–C(3)	1.74(1)
Fe–S(5)	2.238(4)	S(6)–C(4)	1.71(1)
Fe–S(6)	2.250(4)	S(7)–C(4)	1.75(1)
Fe–S(10)	2.242(4)	S(7)–C(5)	1.76(1)
S(1)–C(1)	1.77(1)	S(8)–C(5)	1.62(1)
S(2)–C(1)	1.72(1)	S(9)–C(5)	1.75(2)
S(2)–C(2)	1.72(1)	S(9)–C(6)	1.75(1)
S(3)–C(2)	1.63(1)	S(10)–C(6)	1.76(1)
S(4)–C(2)	1.75(1)	C(1)–C(3)	1.35(2)
S(4)–C(3)	1.72(1)	C(4)–C(6)	1.36(2)
S(1)–Fe–S(5)	90.2(1)	Fe–S(10)–C(6)	102.1(5)
S(1)–Fe–S(6)	85.8(1)	S(1)–C(1)–C(3)	120(1)
S(5)–Fe–S(10)	89.0(2)	S(2)–C(1)–C(3)	118(1)
S(6)–Fe–S(10)	90.4(2)	S(2)–C(2)–S(4)	111.8(8)
C(1)–S(2)–C(2)	97.6(6)	S(5)–C(3)–C(1)	122(1)
C(2)–S(4)–C(3)	97.9(6)	S(6)–C(4)–C(6)	122(1)
Fe–S(5)–C(3)	103.6(5)	S(7)–C(4)–C(6)	115(1)
Fe–S(6)–C(4)	102.6(5)	S(7)–C(5)–S(9)	110.7(8)
C(4)–S(7)–C(5)	99.3(7)	S(9)–C(6)–C(4)	117(1)
C(5)–S(9)–C(6)	98.3(8)	S(10)–C(6)–C(4)	121(1)

3.164(3) Å]. These findings are almost the same as for complex **1**. Within the dimeric unit there are some S···S contacts (3.47–3.62 Å) within the sum (3.7 Å) of their van der Waals radii. The dimeric units of the anions approach each other through weak S···S contacts of 3.86–3.93 Å, forming a one-dimensional chain approximately parallel to the (110) plane (Fig. 4), as observed for complex **1**.

Spectroscopic and Oxidation Properties of the $[Fe(C_3S_5)_2]^-$ *and* $[Fe(C_3Se_5)_2]^-$ *Complexes.*—The electronic absorption spectra of complex **1** in a variety of solvents and its powder reflectance spectrum are illustrated in Fig. 5. Intense bands at 381 and 468 nm in the absorption spectrum in acetonitrile are ascribed to ligand π–π* transitions.[26] As was reported for some bis(1,2-dithiolato)iron(III) complexes,[5] the anions of complex **1** are likely to be dimerized in acetonitrile. The band at 760 nm observed in this solvent corresponds to the reflection band at 760 nm due to the dimerized anion species. However, this band disappears in solvents having higher co-ordinating ability such as dimethylformamide, dimethyl sulfoxide and pyridine, which may indicate the dissociation of the dimerized anions into monomer units.

Fig. 6 shows the electronic absorption spectra of complex **5** in same solvents, together with the powder reflectance spectrum. The reflectance band at 730 nm is also ascribed to the dimerized anion moiety. The band occurs at a shorter wavelength than for the corresponding band of complex **1**. The electronic absorption spectra in solution exhibit no bands due to the dimerized anion species. This finding indicates that the dimerized form of the anion of complex **5** is less stabilized than that of **1**. This is consistent with the occurrence of a broad ESR signal of complex **5** (see Fig. 7) in the solid state, which is in contrast to the absence of a signal of complex **1** at both room temperature and 77 K owing to strong antiferromagnetic Fe···Fe interactions.

Cyclic voltammograms of the $[Fe(C_3S_5)_2]^-$ and $[Fe(C_3Se_5)_2]^-$ anions in dimethylformamide are shown in Fig. 8. Both the anion species exhibit the reversible redox process $[Fe(C_3X_5)_2]^{2-}$–$[Fe(C_3X_5)_2]^-$ (X = S or Se) at $E^\circ_{\frac{1}{2}}$ −0.43 V (*vs.*

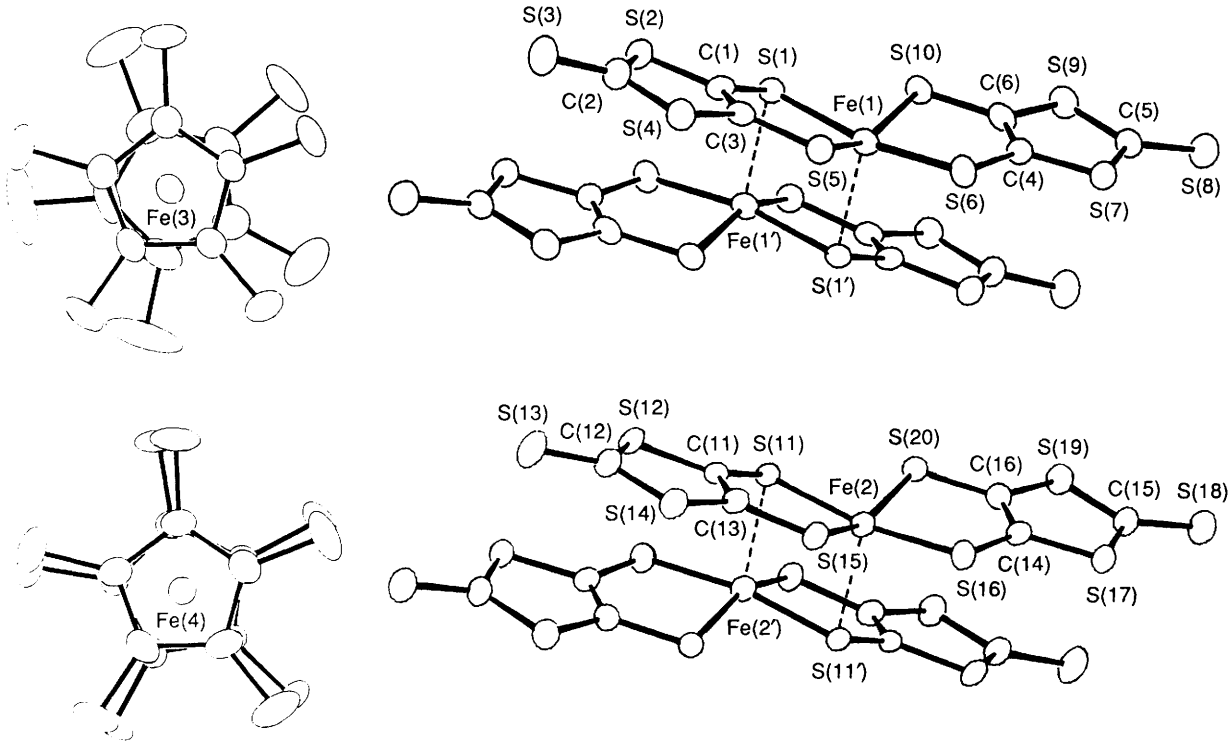

Fig. 3 Geometries of the $[Fe(C_5Me_5)_2]^+$ cations and the dimerized $[Fe(C_3S_5)_2]^-$ anions of $[Fe(C_5Me_5)_2][Fe(C_3S_5)_2]$ **4**, together with the atom-labelling scheme

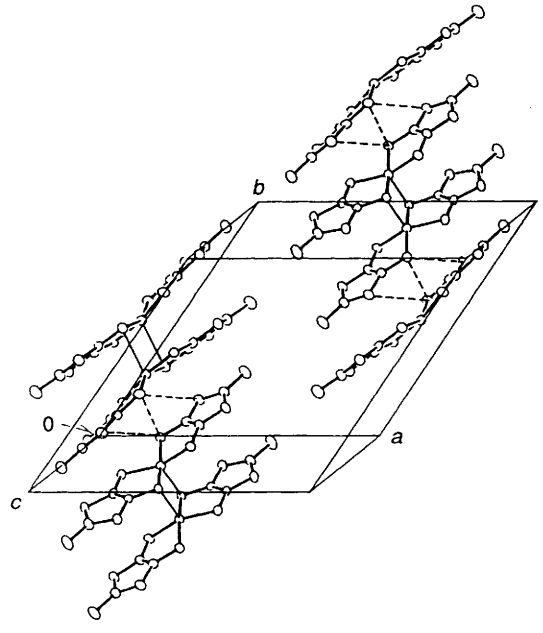

Fig. 4 Packing diagram of the anions of $[Fe(C_5Me_5)_2][Fe(C_3S_5)_2]$ **4**; dashed lines represent non-bonded S ··· S contacts less than 4.0 Å

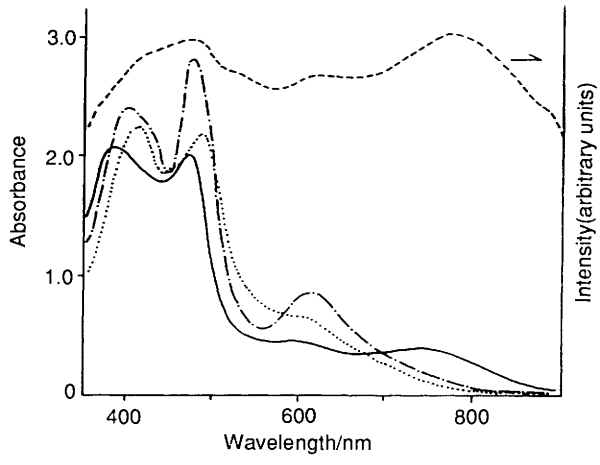

Fig. 5 Electronic absorption spectra of $[NBu^n_4][Fe(C_3S_5)_2]$ **1** (1.4×10^{-4} mol dm^{-3}) in acetonitrile (——), dimethylformamide (· · · ·) and pyridine (– · – · –) and its powder reflectance spectrum (– – – –)

SCE). Oxidation peak potentials at +0.14 and +0.28 V (*vs.* SCE) observed for the sulfur analogue correspond to oxidation processes of the $[Fe(C_3S_5)_2]^-$ and $[Fe(C_3S_5)_2]^0$ species, respectively. Corresponding oxidation peak potentials of the selenium analogue occur at −0.08 and +0.29 V. The first oxidation potential of the selenium analogue is 0.22 V lower than that of the sulfur one. This behaviour is similar to the finding that oxidation potentials of $[M(C_3Se_5)_2]^{n-}$–$[M(C_3Se_5)_2]^{(n-1)-}$ couples are 0.06–0.39 V lower than those of $[M(C_3S_5)_2]^{n-}$–$[M(C_3S_5)_2]^{(n-1)-}$ (M = Ni^{II} or Pd^{II}; n = 2;[32] Au^{III}, n = 1[11]).

Oxidized $[Fe(C_3X_5)_2]^{n-}$ (X = S or Se; n < 1) *Complexes.*—Partial oxidation of the $[Fe(C_3S_5)_2]^-$ complexes occurs upon reaction with iodine or the $[Fe(C_5H_5)_2]^+$ cation, or by electrolysis. The $[Fe(C_3Se_5)_2]^-$ complexes are also oxidized by the $ttf^{\cdot+}$ radical cation and the $[Fe(C_5Me_5)_2]^+$ cations as well as by the above oxidizing agents. These findings are consistent with the fact that the $[Fe(C_3Se_5)_2]^-$ anion is oxidized at a lower potential than is the $[Fe(C_3S_5)_2]^-$ anion.

Table 7 summarizes binding energies of Fe $2p_{\frac{3}{2}}$ electrons of the iron(III) complexes determined by XPS, together with the ν(C=C) stretching IR frequencies of the ligands and their electrical conductivities. The values of the binding energies of the oxidized $[Fe(C_3Se_5)_2]^{n-}$ complexes are almost the same as that of the unoxidized $[Fe(C_3Se_5)_2]^-$ species. This indicates ligand-centred oxidation, as was observed for oxidized $[M(C_3S_5)_2]^{n-}$ (M = Ni^{II}, Pd^{II} or Pt^{II}; n < 2)[32] and $[Au(C_3X_5)_2]^{n-}$ (X = S or Se; n < 1) complexes.[11] The oxidized $[Fe(C_3S_5)_2]^{n-}$

Table 6 Selected bond lengths (Å) and angles (°) with e.s.d.s in parentheses for $[Fe(C_5Me_5)_2][Fe(C_3S_5)_2]$ **4**

Fe–S(1)	2.254(4)	S(9)–C(6)	1.72(1)
Fe–S(5)	2.236(3)	S(10)–C(6)	1.76(1)
Fe–S(6)	2.240(4)	S(11)–C(11)	1.73(1)
Fe–S(10)	2.237(3)	S(12)–C(11)	1.770(9)
Fe–S(11)	2.241(3)	S(12)–C(12)	1.73(1)
Fe–S(15)	2.242(4)	S(13)–C(12)	1.64(1)
Fe–S(16)	2.239(4)	S(14)–C(12)	1.741(8)
Fe–S(20)	2.240(3)	S(14)–C(13)	1.73(1)
S(1)–C(1)	1.74(1)	S(15)–C(13)	1.734(9)
S(2)–C(1)	1.75(1)	S(16)–C(14)	1.746(9)
S(2)–C(2)	1.75(1)	S(17)–C(14)	1.74(1)
S(3)–C(2)	1.64(1)	S(17)–C(15)	1.722(8)
S(4)–C(2)	1.73(1)	S(18)–C(15)	1.66(1)
S(4)–C(3)	1.74(1)	S(19)–C(15)	1.73(1)
S(5)–C(3)	1.74(1)	S(19)–C(16)	1.75(1)
S(6)–C(4)	1.73(1)	S(20)–C(16)	1.73(1)
S(7)–C(4)	1.74(1)	C(1)–C(3)	1.35(1)
S(7)–C(5)	1.737(9)	C(4)–C(6)	1.35(1)
S(8)–C(5)	1.63(1)	C(11)–C(13)	1.34(1)
S(9)–C(5)	1.74(1)	C(14)–C(16)	1.35(1)
Fe(3)–C(21–30)	2.066–2.116 (av. 2.090)		
Fe(4)–C(31–40)	2.082–2.110 (av. 2.099)		
C–C(21–30)	1.40–1.46 (av. 1.42)		
C–C(41–50)	1.42–1.45 (av. 1.43)		
C–CH_3(21–30,31–40)	1.51–1.55 (av. 1.53)		
C–CH_3(41–50,51–61)	1.49–1.53 (av. 1.52)		

S(1)–Fe(1)–S(5)	90.6(1)	Fe(2)–S(11)–C(11)	102.5(2)
S(1)–Fe(1)–S(10)	86.3(1)	Fe(2)–S(15)–C(13)	102.5(4)
S(5)–Fe(1)–S(6)	87.5(1)	Fe(2)–S(16)–C(14)	101.7(4)
S(6)–Fe(1)–S(10)	90.5(1)	Fe(2)–S(20)–C(16)	101.9(3)
S(11)–Fe(2)–S(15)	90.6(1)	S(1)–C(1)–C(3)	121.5(9)
S(11)–Fe(2)–S(16)	85.2(1)	S(5)–C(3)–C(1)	122.6(8)
S(15)–Fe(2)–S(20)	89.1(1)	S(6)–C(4)–C(6)	122.8(9)
S(16)–Fe(2)–S(20)	90.8(1)	S(10)–C(6)–C(4)	120.4(8)
Fe(1)–S(1)–C(1)	102.6(4)	S(11)–C(11)–C(13)	122.3(7)
Fe(1)–S(5)–C(3)	102.6(3)	S(15)–C(13)–C(11)	121.9(9)
Fe(1)–S(6)–C(4)	102.2(4)	S(16)–C(14)–C(16)	121.7(10)
Fe(1)–S(10)–C(6)	102.4(3)	S(20)–C(16)–C(14)	122.1(8)

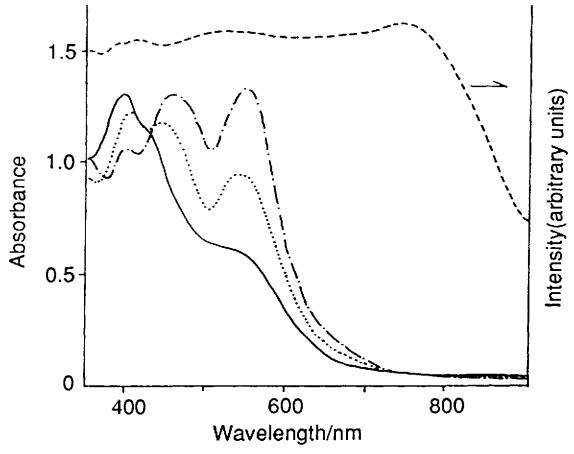

Fig. 6 Electronic absorption spectra of $[NBu^n_4][Fe(C_3Se_5)_2]$ **5** (8.7×10^{-5} mol dm^{-3}) in acetonitrile (——), dimethylformamide (· · · ·) and pyridine (– · – · –) and its powder reflectance spectrum (– – – –)

($n < 1$) complexes have also similar binding energies of the Fe $2p_{\frac{3}{2}}$ electrons to those of the selenium analogues. However, the unoxidized $[Fe(C_3S_5)_2]^-$ species exhibit lower binding energies. Although the central metal is essentially in the iron(III) state, the anion moieties are dimerized through Fe–S linkages. This strong Fe–S interaction as well as the difference in geometry around the iron(III) ion may result in appreciable lowering of the binding energy. The oxidized $[Fe(C_3S_5)_2]^{n-}$ species seem to assume a monomeric geometry.

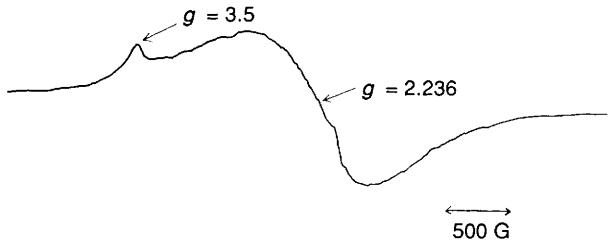

Fig. 7 The ESR spectrum of $[NBu^n_4][Fe(C_3Se_5)_2]$ **5** in the solid state at 77 K; G = 10^{-4} T

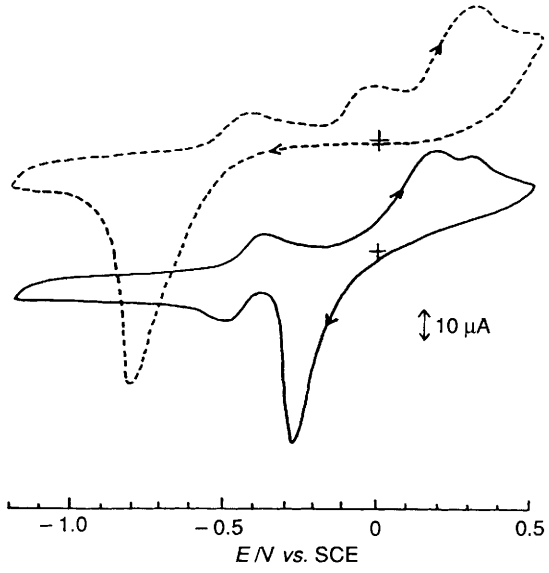

Fig. 8 Cyclic voltammograms of $[NBu^n_4][Fe(C_3S_5)_2]$ **1** (——) and $[NBu^n_4][Fe(C_3Se_5)_2]$ **5** (1.0×10^{-3} mol dm^{-3}) in dimethylformamide (– – – –), 0.1 mol dm^{-3} $[NBu^n_4][ClO_4]$; scan rate, 0.1 V s^{-1}

Table 7 Binding energies (E_b) of Fe $2p_{\frac{3}{2}}$ electrons determined by X-ray photoelectron spectroscopy, the ν(C=C) stretching IR frequencies of the C_3X_5 ligands (X = S or Se) and room-temperature electrical conductivities (σ) of the iron complexes

Complex	E_b/eV	ν(C=C)/cm^{-1}	σ/S cm^{-1}
1	708.7	1438	5.9×10^{-7}
3	708.4	1353	5.8×10^{-2}
4	708.9	1435	6.7×10^{-7}
5	710.5	1435	5.9×10^{-8}
7		1390	1.9×10^{-5}
8	710.0	1370	1.6×10^{-3}
9	710.9	1380	2.9×10^{-2}
10		1390	4.0×10^{-5}
11	710.9	1350	1.5×10^{-6}
12	710.8	1363	1.9×10^{-5}
13	710.9	1360	1.0×10^{-1}
14	709.2	1350	1.3×10^{-2}

In accordance with these ligand-centred oxidations of $[Fe(C_3X_5)_2]^{n-}$ (X = S or Se) complexes, the oxidized species show the C=C stretching IR bands of the ligands at lower wavenumbers (1350–1390 cm^{-1}) compared with the unoxidized $[Fe(C_3X_5)_2]^-$ (X = S or Se) complexes (1438 and 1435 cm^{-1}, respectively). This is the same as found for $[Ni(C_3S_5)_2]^{n-}$ ($0 < n < 2$)[32] and $[Au(C_3X_5)_2]^{n-}$ (X = S or Se; $0 < n < 1$) complexes.[11]

Electrical conductivities measured at room temperature for compacted pellets are listed in Table 7. Complexes **1** and **5** have very low conductivities. The oxidized complexes, however, exhibit higher conductivities as previously reported for $[NBu^n_4]_{0.05}[Fe(C_3S_5)_2]$.[9] Complex **13** in particular, prepared

by electrolysis, shows an extremely high conductivity, which seems to arise from the formation of effective conduction pathways through S • • • S contacts. Powder reflectance spectra of these oxidized species show broad bands around 900 nm ascribed to intermolecular interactions. In complex **3** containing the $ttf^{\bullet+}$ radical cation, the anion is not oxidized formally but nevertheless shows a considerably high conductivity, as reported previously.[9] The ESR spectrum of **3** shows a sharp signal ($g = 2.007$) of the $ttf^{\bullet+}$ radical cation and a broad signal due to the oxidized $[Fe(C_3S_5)_2]^-$ anion. The ν(C=C) stretching frequency of the ligand occurs at 1353 cm^{-1}, suggesting ligand-centred oxidation. These findings suggest some charge transfer between the anion and the cation, leading to the formation of conduction pathways constructed from both the anions and the cations. Although selenium has more extended orbitals and a higher polarizability than sulfur, the $[Fe(C_3Se_5)_2]^{n-}$ ($n < 1$) complexes exhibit lower conductivities compared with the $[Fe(C_3S_5)_2]^{n-}$ ($n < 1$) species owing to less effective molecular interactions through Se • • • Se non-bonded contacts in the solid state.

Acknowledgements

We thank Professor K. Nakatsu of Kwansei Gakuin University, Nishinomiya, for the use of the programs for the X-ray structure analysis. This work was supported by a Grant-in-Aid for Scientific Research on Priority Areas No. 02230220 from the Ministry of Education, Science and Culture, Japan.

References

1 G. Matsubayashi, *Rev. Heteroatom Chem.*, (Myu, Tokyo), 1991, **4**, 171.
2 P. Cassoux, L. Valade, H. Kobayashi, A. Kobayashi, R. A. Clark and A. E. Underhill, *Coord. Chem. Rev.*, 1991, **110**, 115.
3 W. C. Hamilton and I. Bernal, *Inorg. Chem.*, 1967, **6**, 2003.
4 M. L. Snow and J. A. Ibers, *Inorg. Chem.*, 1973, **12**, 249.
5 M. G. Kanatzidis and D. Coucouvanis, *Inorg. Chem.*, 1984, **23**, 403.
6 S. Alvartz, R. Vicente and R. Hoffmann, *J. Am. Chem. Soc.*, 1985, **107**, 6253.
7 D. T. Sawyer, G. S. Srivatsa, M. E. Bodini, W. P. Schaefer and R. M. Wing, *J. Am. Chem. Soc.*, 1986, **108**, 936.
8 F. Kubel, L. Valade, J. Strahle and P. Cassoux, *C.R. Hebd. Seances Acad., Ser. 2*, 1982, **295**, 179.
9 F. Kubel, J. Strahle and P. Cassoux, *J. Phys. Colloq.*, 1983, **44**, C3-1265.
10 H. Poleschner, E. Fanghanel and H. Mehner, *J. Prakt. Chem.*, 1981, **323**, 919.
11 G. Matsubayashi and A. Yokozawa, *J. Chem. Soc., Dalton Trans.*, 1990, 3013, 3535.
12 G. Steimecke, H. J. Sietler, R. Kirmse and E. Hoyer, *Phosphorus Sulfur*, 1979, **7**, 49.
13 F. Wudl, *J. Am. Chem. Soc.*, 1975, **97**, 1962.
14 A. Yokozawa and G. Matsubayashi, *Inorg. Chim. Acta*, 1991, **186**, 165.
15 G. Matsubayashi and K. Akiba, *J. Chem. Soc., Dalton Trans.*, 1990, 115.
16 K. Ueyama, G. Matsubayashi and T. Tanaka, *Inorg. Chim. Acta*, 1984, **87**, 143.
17 G. Matsubayashi, S. Tanaka and A. Yokozawa, *J. Chem. Soc., Dalton Trans.*, 1992, 1827.
18 T. Nojo, G. Matsubayashi and T. Tanaka, *Inorg. Chim. Acta*, 1989, **159**, 49.
19 A. C. T. North, D. C. Phillips and F. C. Matheus, *Acta Crystallogr., Sect. A*, 1968, **4**, 351.
20 C. J. Gilmore, MITHRIL: an integrated direct methods computer program, *J. Appl. Crystallogr.*, 1984, **17**, 42; P. T. Beurskens, DIRDIF: direct methods for difference structures—an automatic procedure for phase extension and refinement of difference structure factors, Technical Report 1984/1 Crystallography Laboratory, Toernooiveld, Nijmegen, 1984.
21 TEXSAN: Structure Analysis Package, Molecular Structure Corporation, College Station, TX, 1985.
22 M. Main, S. E. Hull, L. Lessinger, G. Germain, J-P. Declerq and M. M. Woolfson, MULTAN 78, A System of Computer Programs for the Automatic Solution of Crystal Structures from X-Ray Diffraction Data, University of York, York, 1978.
23 *International Tables for X-Ray Crystallography*, Kynoch Press, Birmingham, 1974, vol. 4.
24 C. K. Johnson, ORTEP II, Report ORNL 5138, Oak Ridge National Laboratory, Tennessee, 1976.
25 A. Yokozawa and G. Matsubayashi, *Inorg. Chim. Acta*, 1992, **193**, 137.
26 G. Matsubayashi, K. Takahashi and T. Tanaka, *J. Chem. Soc., Dalton Trans.*, 1988, 967.
27 J. S. Miller, J. C. Calabrese, H. Rommelmann, S. R. Chittipeddi, M. A. Reiff and A. J. Epstein, *J. Am. Chem. Soc.*, 1987, **109**, 769.
28 J. S. Miller, J. H. Zhang and W. M. Reiff, *J. Am. Chem. Soc.*, 1987, **109**, 4584.
29 E. Gerbert, A. H. Reis, jun., J. S. Miller, H. Rommelmann and A. J. Epstein, *J. Am. Chem. Soc.*, 1982, **104**, 4403.
30 J. S. Miller, J. C. Calabrese, R. L. Harlow, D. A. Dixon, J. H. Zhang, W. M. Reiff, S. Chittipeddi, M. A. Selover and A. J. Epstein, *J. Am. Chem. Soc.*, 1990, **112**, 5496.
31 D. P. Freyberg, J. L. Robbins, K. N. Raymond and J. C. Smart, *J. Am. Chem. Soc.*, 1979, **101**, 892.
32 Y. Sakamoto, G. Matsubayashi and T. Tanaka, *Inorg. Chim. Acta*, 1986, **113**, 137.

Received 13*th April* 1992; *Paper* 2/01913B